In the present study, we elucidate the thickness limitation of layered cell sheets and attempted to overcome this limitation by a multistep transplantation procedure. In addition, we demonstrate a new therapeutic strategy to transplant multilayer grafts ectopically fabricated with a surgically connectable artery and vein.

MATERIALS AND METHODS

All animal experiments were performed in accordance with the "Guidelines of Tokyo Women's Medical University on Animal Use."

Temperature-responsive culture surfaces

Specific procedures for preparation of square-geometry PIPAAm-grafted cell culture dishes have been described previously (29). Briefly, IPAAm monomer (kindly provided by Kohjin, Tokyo, Japan) in 2-propanol solution was spread onto commercial tissue culture polystyrene dishes. These dishes were then subjected to irradiation (0.25 MGy electron beam dose) using an Area Beam Electron Processing System (Nisshin High Voltage, Kyoto, Japan), resulting in polymerization and covalent bonding of IPAAm to the dish surface. These PIPAAm-grafted dishes were rinsed with cold distilled water to remove ungrafted IPAAm and dried in nitrogen gas. Next, the PIPAAm-grafted surface was masked with a square glass coverslip (24×24 mm, Matsunami, Osaka, Japan) and acrylamide (AAm) monomer (Wako Pure Chemicals, Tokyo, Japan) solution in 2-propanol was spread onto the masked dish surface. Then, the dish surface was irradiated in the same manner. The resulting culture dishes had center square areas grafted with temperature-responsive PIPAAm with a surrounding border of non cell-adhesive poly-AAm. Culture dishes were finally gas sterilized by ethylene oxide.

Primary culture of neonatal rat cardiomyocytes

Ventricles from 1-day-old Wistar rats (Nisseizai, Tokyo, Japan) were digested at 37°C in Hank's solution (Sigma, St. Louis, MO) containing collagenase (class II, Worthington Biochemical, Lakewood, NJ). Isolated cells were suspended in the culture medium comprising 6% FBS (Moregate Biotech, Bulimba, QLD, Australia), 40% Medium 199 (Invitrogen, Carisbad, CA), 0.8% penicillin-streptomycin solution (Wako Pure Chemicals), 2.7 mM glucose, and 54% balanced salt solution containing 116 mM NaCl, 1.0 mM NaH_2PO_4, 0.8 mM $MgSO_4$, 1.18 mM KCl, 0.87 mM $CaCl_2$, and 26.2 mM $NaHCO_3$. Cell suspensions were plated at a density of 4.8×10^6 cells per square-geometry PIPAAm grafted dish and incubated at 37°C in a humidified atmosphere with 5% CO_2. For green fluorescent protein (GFP)-positive cardiomyocytes, ventricles were isolated from GFP-positive SD neonatal rats (SD TgN (act-EGFP) OsbCZ-004), which were kindly provided by Masaru Okabe.

Fabrication of myocardial tissue grafts

Neonatal rat cardiomyocytes were cultured to confluency for 4 days at 37°C on square-designed temperature responsive dishes. The culture dishes were set in another CO_2 incubator set at 20°C to release confluent cells as contiguous cell sheets without enzyme treatment. Cardiomyocyte sheets detached spontaneously within 1 h and became slightly shrunken to ~1 cm square cell sheets due to cytoskeletal reorganization and sheet lateral traction forces. The entire cell sheet with media was gently aspirated into the tip of a pipette and the first sheet was transferred again onto the

temperature responsive culture surfaces with fresh media dropped onto the sheet to spread folded portions. After sheet spreading, media was aspirated and the dish was incubated at 37°C to allow the cell sheet to fully adhere to the culture surface. To layer cell sheets, another cardiomyocyte sheet, detached from a PIPAAm-grafted dish, was transferred and stacked onto the first cell sheet in the same fashion. Identical procedures were repeated to layer additional sheets in vitro.

Transplantation of engineered myocardial tissue grafts

Male F344 nude rats (4–6 wk old) were anesthetized with intraperitoneal injections of sodium pentobarbital (30 mg/kg). An L-shaped incision (~3×2 cm) was made in the dorsal skin and lifting of the incised skin exposed the underlying tissue. Cardiomyocyte sheets (1–6 sheets, each n=4) stacked on PIPAAm-grafted surfaces were detached again by lowering the culture temperature, and washed with Hank's solution. The cell constructs were lifted on top of a sterile polypropylene support sheet (2×1.5 cm) and transplanted onto dorsal subcutaneous tissues by sliding from the nonadhesive polypropylene sheet. The transplants were covered with 0.5 mm thick silicone membranes (Unique Medical, Tokyo, Japan) to prevent adhesion to the skin and the incisions were closed with 7-0 nylon sutures. For multistep transplantation procedures, triple-layer constructs were repeatedly transplanted at 1, 2, or 3 day intervals (double-step procedure: n=16, 10-times procedure: n=5). For each step, the silicone membranes were removed and then replaced after each transplant procedure. At the appropriate time after these procedures, the rats were anesthetized as described previously, and physiological and morphological analyses were performed. Rats were then killed with over-doses of pentobarbital.

Engineering vessel-accessible constructs and their ectopic transplantation

Male F344 nude rats (7–8 wk old) were anesthetized and the femoral skin was cut and opened. A superficial caudal epigastric artery and vein, branches of the femoral artery and vein, were then exposed. Two triple-layer myocardial tissue grafts were transplanted at a 1 day interval, over an area that included the artery and vein that was relatively smooth, using the same procedures as used for dorsal subcutaneous tissue implantation (n=13). Two weeks after the procedure, the constructs were resected together with the femoral artery and vein under anesthesia and heparinization (400 IU/kg, intravenous injection), and the peripheries of the femoral vessels were then ligated. To examine blood perfusion within the excised construct via the artery and vein, Indian ink was injected from the inlet of the femoral artery and the entire construct was then fixed (n=4). To pursue the possibility of ectopic transplantation, surgically resected constructs were immediately immersed in cold lactated Ringer's solution (n=4). Separate nude rats (9–10 wk old) were then anesthetized and skin incisions were made in the neck to expose the underlying tissue. The common carotid artery and the jugular vein were exposed and isolated from their peripheries and then clamped to prevent subsequent bleeding. The femoral vessels of engineered constructs were connected to neck vessels by a cuff technique as previously reported (30). Briefly, the femoral artery and vein were introduced into 22 and 21 gauge cuffs, respectively, and were everted and secured with circumferential 6-0 silk sutures. The carotid artery and the jugular vein were gently slipped over the cuff that had been fixed to the femoral artery and vein and again secured again with circumferential 6-0 silk sutures. After the clamps had been removed and graft beating was confirmed, the incision was closed. After graft survival was examined for 2 wk, the constructs were fixed and the rats were killed.

Histological analysis

For cross-sectional observations, resected grafts were fixed with formalin, embedded in paraffin, and sagittal-sectioned into 10 μm slices. Azan staining was performed by conventional methods. The thickness of the engineered constructs was measured using 5 cross-sectional microscopic images for each graft.

For immunohistochemistry, paraffin-embedded sections were incubated with either a 1/200 dilution of mouse anti-connexin 43 (Chemicon International, Temecula, CA) or a 1/200 dilution of mouse anti-troponin T, cardiac isoform (NeoMarkers, Fremont, CA) monoclonal antibodies at 4°C overnight in a moist chamber. Sections were then washed with PBS and incubated with a 1/200 dilution of Alexa Fluor® 488-labeled goat anti-mouse IgG antibodies (Molecular Probes, Eugene, OR) for 2 h at room temperature. Sections were finally counter-stained with a 1/500 dilution of the DNA binding dye Hoechst 33342 (Sigma) to visualize cell nuclei and observed using confocal laser scanning microscopy (TCS-SP, Leica Microsystems AG, Wetzlar, Germany).

Transmission electron microscopy

Resected tissues were prefixed with 4% paraformaldehyde for 1 h, fixed with 2% glutaraldehyde overnight, and then postfixed with 2% osmium tetroxide for 3 h. The samples were dehydrated through a graded series of ethanol and embedded using EPON812. Ultrathin sections (80–90 nm) stained with uranyl acetate and lead citrate, were examined at 85 kV by transmission electron microscopy (TEM; JEM2000EX, JEOL, Tokyo, Japan).

Electrophysiological analysis

To detect electrical potentials in overlaid triple-layer constructs separately, two grafts were transplanted with a partial overlap. One month after the procedure, the transplantation site was opened under anesthesia, and two microelectrodes (100 μm in diameter, Unique Medical) were positioned over a nonoverlapping portion of each graft. Electrical potentials were amplified by bioelectric amplifiers (UA102, Unique Medical) and recorded using a data acquisition system (NR-2000, Keyence, Osaka, Japan). For electrical propagation analysis, a stimulation bipolar electrode (TF200-029, Unique Medical) was set at the edge of one graft, and monophasic pacing pulses (2–4 Hz, 5 ms, 2–3 V) were applied by an electrical stimulator (UPS-801, Unique Medical).

Video capture

Macroscopic images of pulsatile myocardial tissue grafts were recorded by a digital video camera (DCR-TRV900, SONY, Tokyo, Japan). The videos were edited with Adobe Premiere Pro software.

Echography

Echograms were recorded with a commercially available echographic system (SSA-550A, Toshiba, Tokyo, Japan) equipped with a 12-MHz transducer (PLM-1202S, Toshiba). Cross-sectional images of the constructs were taken under anesthesia and graft thickness was measured in the diastolic period.

Data analysis

Data are expressed as mean ± SD. Statistical analysis was performed by use of a Student's unpaired *t* test. A *P* value of <0.05 was considered significant.

RESULTS

Primary ischemia limits layered-cell-sheet thickness

To examine the thickness limitation of layered cell sheets, an increasing number (1–5) of neonatal rat cardiomyocyte sheets, all released from PIPAAm-grafted dishes, were layered in vitro and transplanted into the dorsal subcutaneous tissue of nude rats. We covered the transplants with silicone membranes to inhibit adhesion of the constructs to the overlying dermal layers, thus allowing host tissue nutrient diffusion only from lower side. One month after the procedure, the sheet constructs were resected and fixed, and the final viable tissue thickness was measured. Azan staining showed that the 1, 2, and 3 layer constructs thoroughly survived without necrosis (Fig. 1*A–C*), but that some parts of the 4 and 5 layer constructs were replaced with disordered vasculature and connective tissue, indicative of necrosis (Fig. 1*D* and *E*). Recovered tissue thickness increased linearly up to the 3-layer construct, but was saturated in the 4 and 5 cell-sheet constructs (25±6, 44±6, 78±14, 80±16, and 82±5 μm thick, respectively) (Fig. 1*F*). Therefore, the thickness limit for layered cardiomyocyte sheets in in vivo subcutaneous tissue appears to be ~80 μm.

Polysurgery overcomes the thickness limitation

We noted that in the process of sheet transplant survival, vascularization within the constructs begins promptly after implantation, creating a well-organized vascular network after a few days in vivo (data not shown). We therefore hypothesized that repeated transplantation of layered cell sheets after intervals that produce sufficient neovascularization within the previously implanted grafts might overcome the limit encountered in bioengineered cell sheet tissue thickness (Fig. 2). To verify this hypothesis, we repeatedly transplanted triple-layer myocardial cell sheet tissue grafts that had, as previously shown, survived primarily only by nutrient diffusion. The two such triple layer grafts were overlaid in rat dorsal subcutaneous tissues at 1, 2, and 3 day intervals to examine the ideal lag-time for the procedures. For reconstruction of spontaneously beating, synchronized, thick tissues capable of myocardial tissue replacement, sufficient electrical communication between the two triple-layer grafts is as critical as sufficient neovascularization. Therefore, electrophysiological and morphological analyses were also performed.

To examine electrical connections between two triple-layer grafts, the second graft was partially overlaid on the first, and the electrical potential of each graft was independently monitored in vivo, with electrodes set on each graft (Fig. 3*A*). One month after the second 3-layer cell-sheet implant procedure, the two overlaid myocardial grafts pulsated spontaneously in the subcutaneous compartment and were completely synchronized when initially transplanted at either 1 or 2 day intervals (Fig. 3*B* and *C*). However, when transplanted at a 3 day interval, the two grafts were electrically dissociated (Fig. 3*D*). Additionally, electrical propagation analyses demonstrated that stimuli to the edge of one graft could be transmitted to the other, when overlaid using the 1 day polysurgery interval (Fig. 3*E* and *F*). Electrical propagation between the two grafts was also

detected when the 2 day interval was used, but no conduction could be observed for the 3 day interval (data not shown). To directly detect pulsations from each of the two overlaid grafts separately, we used a tissue marking system where the first triple-layer graft was engineered from neonatal rat cardiomyocytes expressing GFP and overlaid with a GFP-negative graft after one day implantation. Although it was impossible to distinguish the two grafts under normal light, the synchronized beating of the GFP-positive graft and the non-fluorescent graft could be detected when both fluorescent and normal illumination were used concurrently (see supplemental video 1).

Histology of the engineered constructs was also examined 1 month postimplantation. Azan stained controls showed significant necrotic tissue within the 6 layer constructs implanted with a single-step procedure (Fig. 4*A*). In contrast, the double-step transplantation of two triple-layer grafts at 1 day intervals permitted whole tissue survival with a well-organized microvascular network. In these cases, the two grafts became intimately connected, resulting in a uniform, cell-dense, thick tissue (Fig. 4*B*), that was consistent with the electrophysiological characterization at this time point. Viable tissues engineered using the 1 day interval implant procedure are significantly thicker than those engineered by single-step transplantation (171±15 vs. 82±5 μm, respectively, $P<0.05$, $n=4$). In the 2 day interval case, the two grafts were substantially separated by in-grown connective tissue, but the grafts remained in direct contact in some areas (Fig. 4*C*). However, with the 3 day interval, grafts were completely separated by thick in-growth of connective tissues (Fig. 4*D*).

Multistep procedures demonstrate ~1 mm thick pulsatile myocardial tissue grafts

These results from both electrophysiological and morphological analyses confirmed our hypothesis and encouraged studies of additional myocardial tissue graft stacking. Therefore, we next repeated the transplantations of triple-layer cell sheet grafts up to 10-times at 1 or 2 day implant intervals. In the case of 10 triple-layer grafts, spontaneous and synchronized graft contraction/relaxation cycles can be macroscopically observed from outside the rat at the subcutaneous implant site (see supplemental video 2). Echocardiography also revealed pulsatile myocardial tissue (see supplemental video 2) with a measured tissue thickness of 0.9 ± 0.1 mm at 1 wk after the final cell sheet implantation procedure ($n=3$). When these transplantation sites were surgically reopened, vigorous graft myocardium-like pulsation was observed (see supplemental video 2), with this beating continuing for several minutes after surgical resection (see supplemental video 3). Azan staining of the grafts created using the 10-times polysurgery technique also showed multilayer thick cell-dense myocardium and well-organized microvessels throughout the transplanted tissues (Fig. 5). When the tissue thickness was measured using fixed cross sections, results showed an average of 0.84 ± 0.16 mm ($n=3$). These findings demonstrated that cell sheet integration has the ability to produce viable, functional myocardial tissue implantable constructs well beyond the current diffusion-limited thickness regime. Additionally, this full retention of electrophysiological and gross tissue behavior represents a potentially valuable new technique for overcoming the vascularization problem in cell-dense tissue engineering.

Transplantation over host vessels realizes surgically accessible grafts

In the clinical replacement of many internal organs, including the heart, direct multistep transplantation of bioengineered tissues may encounter difficulties because each individual procedure has a relatively high risk of complications. Alternatively, ectopic fabrication of viable, thick tissues and their transplantation into target organs may alleviate such complications. Our experiments show that thick cell-dense tissues can be successfully bioengineered within subcutaneous sites with requisite vasculogenesis likely induced from the surrounding host tissue. However, it is technically impossible to surgically cut and reconnect the host microvasculature ectopically to developing vessels within the target tissues. Therefore, the ectopic constructs must be accompanied by surgically accessible, durable arterial and venous conduits. To overcome this obstacle, we hypothesized that repeated transplantation of layered cell sheets over an existing host large artery and vein might promote blood perfusion throughout the entire construct, thus inducing vascularization by the host into the implant, and creating a construct accompanied by surgically accessible vessels (Fig. 6). To verify this hypothesis in a small animal model, the femoral artery and vein were selected as candidates for host blood vessels. Triple-layer cardiomyocyte sheets were repeatedly transplanted over an exposed superficial caudal epigastric artery and vein, branches of the femoral artery and vein, in the leg of a nude rat with the 1 day interval procedure. When transplantation sites were opened 2 wk after this procedure, the grafts pulsated strongly and synchronously over the vessels (see supplemental video 4). To examine blood perfusion within the construct via the selected host artery and vein, we resected the constructs together with the femoral artery and vein. Indian ink was then infused from the inlet of the femoral artery. Results show that the ink first flowed in through the femoral artery and the superficial caudal epigastric artery, and then diffused into the explanted bioengineered graft (see supplemental video 4). The ink was finally discharged from the explant via the femoral vein and through the superficial caudal epigastric vein. Cross sections of ink-perfused myocardial tissue grafts showed that the entire vascular network within the grafts was stained with the black ink, indicating vasculogenesis induced from the host and that blood supply was indeed from the selected artery (Fig. 7*A*, *B*), confirming our second hypothesis.

Immunohistochemical analysis of double-step myocardial tissue grafts showed diffuse connexin 43 staining throughout the thick tissue grafts, indicating the likely presence of gap junctions that allow for observed electrical communication between the cardiomyocytes of the bioengineered grafts (Fig. 7*C*). Anti-troponin T antibody staining demonstrated diffuse and disorganized staining at 3 days after transplantation, but that sarcomeres had developed and were well organized at 7 days (Fig. 7*D* and *E*). Additionally, transmission electron microscopy of the myocardial tissue grafts showed characteristic structures of normal cardiac muscle such as myofilaments and intercalated disks (Fig. 7*F*).

Surgically accessible grafts survive after ectopic transplantation

Finally, we examined the possibility of ectopic transplantation of the bioengineered tissues. We resected a similar multilayer construct from the leg of a nude rat, with the connectable host artery and vein, and then transplanted the graft into the neck of another nude rat. The protruding femoral artery and vein of the implant were then connected to the carotid artery and the jugular vein respectively, in the new host. When the grafts were reperfused, they began to pulsate spontaneously after a few seconds (see supplemental video 4). These grafts survived and

maintained their characteristic beating 2 wk after the procedure, demonstrating the clinical potential of the application of transplanting ectopically bioengineered tissues.

DISCUSSION

While previous studies have demonstrated the survival of implanted tissue engineered cardiac grafts, (13, 31) the limits on passive diffusion have thus far prevented the creation of thick, viable tissues. Indeed, using our method of cell sheet engineering, four-layer myocardial constructs were able to recreate cell-dense pulsatile tissues, yet core ischemia within the grafts restricts the number of cell sheets that could be effectively layered. (28)

In the present study, we have successfully fabricated cell-dense full-thickness tissues using polysurgery of cultured cell sheets. Direct attachment of triple-layer myocardial grafts, also fabricated by the direct stacking of confluent cell sheets, leads to such cell-dense, thick and viable tissues. Electrical and morphological communication between the two myocardial tissue grafts rapidly and completely establishes with this tandem cell sheet transplantation at intervals of <2 days. Direct cell-to-cell communication between the integrated cardiomyocyte sheets enables electrical synchronization and facilitates spontaneous and simultaneous pulsation in the recreated myocardial tissues. On the other hand, the encapsulation tissue, initially formed over the first graft in the 3 day interval case, is believed to inhibit electrical conductivity between the layered grafts, results that are supported by the electrophysiological decoupling observed for this case.

Regarding possibilities for the scale-up of engineered tissues for more extensive use, many challenges remain to overcome endemic tissue vascularization problems. One major obstacle is the question of how to fabricate microvascular networks within bioengineered cell-dense constructs. In the transplantation of cell-dense tissues lacking a preformed microvasculature, survival tissue thickness is mass-transport limited to gases (e.g., oxygen and carbon dioxide), fluids, and dissolved metabolites. Cell necrosis thus occurs well-before requisite vascular networks can develop within the inner portions of the implanted tissue where nutrient diffusion is insufficient. Growth factor administration, gene transfer and coculture of vascular progenitor cells may accelerate vascular growth and contribute to the fabrication of thicker tissues to some extent. Nevertheless, such strategies are presently unable to rapidly perfuse thick implanted, cell-dense transplants sufficiently to avoid hypoxia and necrosis. Other researchers have also attempted to engineer vascularized tissues by prefabricating vascular networks in vitro (32, 33); however, further studies are still needed to develop techniques for culturing selected cell types three-dimensionally. Additionally, the question of whether the engineered vasculature is a truly efficient and effective functional network for maintaining tissue survival also needs to be clarified. If we consider developmental stages in vivo, microvascular networks are prompted to form in accordance with concomitant surrounding tissue growth. Therefore, the simultaneous reconstruction of tissues together with their own vascular networks may be a crucial factor for cell-dense tissue engineering. In this regard, the present step-by-step polysurgery approach based on cell sheet integration appears feasible for fabricating viable, thick tissues with appropriate vascular network formation and without mass transport limitations.

Most tissue-engineered transplants without direct vascular networks and anastomoses must rely on either passive perfusion/diffusion transport of nutrients from the surrounding host tissue in acute posttransplant phases or induced vasculogenesis from the host via multiple connecting

microvascular in-growths in chronic phases. However, in the present study, we have fabricated viable thick tissues perfused via surgically accessible and connectable blood vessels by using an existing host artery and vein at the implant site. This approach permits the successful transplantation of ectopically bioengineered cell-dense tissues via direct in-grown vessel anastomoses, for the first time. This in vivo tissue engineering application is general and applicable to many tissues types beyond the myocardial model demonstrated here, and should thus contribute to further advances and, hopefully, the effective repair of various tissues, including the myocardium.

In conclusion, polysurgery of cultured, layered cell sheets is shown to produce thick, functional, cell-dense myocardium in rat dorsal subcutaneous tissues, overcoming mass transport limitations commonly encountered due to acute insufficient vascularization post-transplantation. In addition, the technique of exploiting existing vessels to induce vascular network perfusion in implanted tissues, demonstrates a further clinical possibility for transplanting ectopically integrated cell sheets via vessel anastomoses. These novel strategies based on cell sheet integration are versatile and should significantly advance the field of tissue engineering.

ACKNOWLEDGMENTS

We appreciate the useful comments and technical criticism from David W. Grainger (Colorado State University). We also thank Masaru Okabe (Genome Information Research Center, Osaka University) for kindly supplying GFP transgenic rats. The present work was supported by grants for the 21COE program and the High-Tech Research Center Program from the Ministry of Education, Culture, Sports, Science, and Technology; the Research Grants for Cardiovascular Disease and Regenerative Medicine from the Ministry of Health, Labor and Welfare; and the Open Research Grant from the Japanese Research Promotion Society for Cardiovascular Diseases.

REFERENCES

1. Langer, R., and Vacanti, J. P. (1993) Tissue engineering. *Science* **260,** 920–926

2. Cao, Y., Vacanti, J. P., Paige, K. T., Upton, J., and Vacanti, C. A. (1997) Transplantation of chondrocytes utilizing a polymer-cell construct to produce tissue-engineered cartilage in the shape of a human ear. *Plast. Reconstr. Surg.* **100,** 297–302 (discussion 303-294)

3. Koh, C. J., and Atala, A. (2004) Tissue engineering, stem cells, and cloning: opportunities for regenerative medicine. *J. Am. Soc. Nephrol.* **15,** 1113–1125

4. Kulig, K. M., and Vacanti, J. P. (2004) Hepatic tissue engineering. *Transpl. Immunol.* **12,** 303–310

5. Nugent, H. M., and Edelman, E. R. (2003) Tissue engineering therapy for cardiovascular disease. *Circ. Res.* **92,** 1068–1078

6. Shin, H., Jo, S., and Mikos, A. G. (2003) Biomimetic materials for tissue engineering. *Biomaterials* **24,** 4353–4364

7. Stock, U. A., and Vacanti, J. P. (2001) Tissue engineering: current state and prospects. *Annu. Rev. Med.* **52,** 443–451

8. Brittberg, M., Lindahl, A., Nilsson, A., Ohlsson, C., Isaksson, O., and Peterson, L. (1994) Treatment of deep cartilage defects in the knee with autologous chondrocyte transplantation. *N. Engl. J. Med.* **331,** 889–895

9. Kirsner, R. S., Falanga, V., and Eaglstein, W. H. (1998) The development of bioengineered skin. *Trends Biotechnol.* **16,** 246–249

10. Shin'oka, T., Imai, Y., and Ikada, Y. (2001) Transplantation of a tissue-engineered pulmonary artery. *N. Engl. J. Med.* **344,** 532–533

11. Leor, J., Aboulafia-Etzion, S., Dar, A., Shapiro, L., Barbash, I. M., Battler, A., Granot, Y., and Cohen, S. (2000) Bioengineered cardiac grafts: A new approach to repair the infarcted myocardium? *Circulation* **102,** III56–III61

12. Papadaki, M., Bursac, N., Langer, R., Merok, J., Vunjak-Novakovic, G., and Freed, L. E. (2001) Tissue engineering of functional cardiac muscle: molecular, structural, and electrophysiological studies. *Am. J. Physiol. Heart Circ. Physiol.* **280,** H168–H178

13. Sakai, T., Li, R. K., Weisel, R. D., Mickle, D. A., Kim, E. T., Jia, Z. Q., and Yau, T. M. (2001) The fate of a tissue-engineered cardiac graft in the right ventricular outflow tract of the rat. *J. Thorac. Cardiovasc. Surg.* **121,** 932–942

14. Zandonella, C. (2003) Tissue engineering: The beat goes on. *Nature* **421,** 884–886

15. Zimmermann, W. H., Schneiderbanger, K., Schubert, P., Didie, M., Munzel, F., Heubach, J. F., Kostin, S., Neuhuber, W. L., and Eschenhagen, T. (2002) Tissue engineering of a differentiated cardiac muscle construct. *Circ. Res.* **90,** 223–230

16. Okano, T., Yamada, N., Sakai, H., and Sakurai, Y. (1993) A novel recovery system for cultured cells using plasma-treated polystyrene dishes grafted with poly(N-isopropylacrylamide). *J. Biomed. Mater. Res.* **27,** 1243–1251

17. Yamada, N., Okano, T., Sakai, H., Karikusa, F., Sawasaki, Y., and Sakurai, Y. (1990) Thermo-responsive polymeric surfaces; control of attachment and detachment of cultured cells. *Makromol. Chem. Rapid Commun.* **11,** 571–576

18. Kushida, A., Yamato, M., Konno, C., Kikuchi, A., Sakurai, Y., and Okano, T. (1999) Decrease in culture temperature releases monolayer endothelial cell sheets together with deposited fibronectin matrix from temperature-responsive culture surfaces. *J. Biomed. Mater. Res.* **45,** 355–362

19. Kushida, A., Yamato, M., Konno, C., Kikuchi, A., Sakurai, Y., and Okano, T. (2000) Temperature-responsive culture dishes allow nonenzymatic harvest of differentiated Madin-Darby canine kidney (MDCK) cell sheets. *J. Biomed. Mater. Res.* **51,** 216–223

20. Harimoto, M., Yamato, M., Hirose, M., Takahashi, C., Isoi, Y., Kikuchi, A., and Okano, T. (2002) Novel approach for achieving double-layered cell sheets co-culture: overlaying endothelial cell sheets onto monolayer hepatocytes utilizing temperature-responsive culture dishes. *J. Biomed. Mater. Res.* **62,** 464–470

21. Kushida, A., Yamato, M., Kikuchi, A., and Okano, T. (2001) Two-dimensional manipulation of differentiated Madin-Darby canine kidney (MDCK) cell sheets: the noninvasive harvest from temperature-responsive culture dishes and transfer to other surfaces. *J. Biomed. Mater. Res.* **54,** 37–46

22. Nishida, K., Yamato, M., Hayashida, Y., Watanabe, K., Maeda, N., Watanabe, H., Yamamoto, K., Nagai, S., Kikuchi, A., Tano, Y., et al. (2004) Functional bioengineered corneal epithelial sheet grafts from corneal stem cells expanded ex vivo on a temperature-responsive cell culture surface. *Transplantation* **77,** 379–385

23. Shimizu, T., Yamato, M., Akutsu, T., Shibata, T., Isoi, Y., Kikuchi, A., Umezu, M., and Okano, T. (2002) Electrically communicating three-dimensional cardiac tissue mimic fabricated by layered cultured cardiomyocyte sheets. *J. Biomed. Mater. Res.* **60,** 110–117

24. Shiroyanagi, Y., Yamato, M., Yamazaki, Y., Toma, H., and Okano, T. (2004) Urothelium regeneration using viable cultured urothelial cell sheets grafted on demucosalized gastric flaps. *BJU Int.* **93,** 1069–1075

25. Yamato, M., Konno, C., Utsumi, M., Kikuchi, A., and Okano, T. (2002) Thermally responsive polymer-grafted surfaces facilitate patterned cell seeding and co-culture. *Biomaterials* **23,** 561–567

26. Nishida, K., Yamato, M., Hayashida, Y., Watanabe, K., Yamamoto, K., Adachi, E., Nagai, S., Kikuchi, A., Maeda, N., Watanabe, H., et al. (2004) Corneal reconstruction with tissue-engineered cell sheets composed of autologous oral mucosal epithelium. *N. Engl. J. Med.* **351,** 1187–1196

27. Shimizu, T., Yamato, M., Kikuchi, A., and Okano, T. (2003) Cell sheet engineering for myocardial tissue reconstruction. *Biomaterials* **24,** 2309–2316

28. Shimizu, T., Yamato, M., Isoi, Y., Akutsu, T., Setomaru, T., Abe, K., Kikuchi, A., Umezu, M., and Okano, T. (2002) Fabrication of pulsatile cardiac tissue grafts using a novel 3-dimensional cell sheet manipulation technique and temperature-responsive cell culture surfaces. *Circ. Res.* **90,** e40–e48

29. Hirose, M., Kwon, O. H., Yamato, M., Kikuchi, A., and Okano, T. (2000) Creation of designed shape cell sheets that are noninvasively harvested and moved onto another surface. *Biomacromolecules* **1,** 377–381

30. Xiu, D., Uchida, H., To, H., Sugimoto, K., Kasahara, K., Nagai, H., Fujimura, A., and Kobayashi, E. (2001) Simplified method of heterotopic rat heart transplantation using the cuff technique: application to sublethal dose protocol of methotrexate on allograft survival. *Microsurgery* **21,** 16–21

31. Zimmermann, W. H., Didie, M., Wasmeier, G. H., Nixdorff, U., Hess, A., Melnychenko, I., Boy, O., Neuhuber, W. L., Weyand, M., and Eschenhagen, T. (2002) Cardiac grafting of engineered heart tissue in syngenic rats. *Circulation* **106,** *Suppl.* 1, I151–I157

32. Kaihara, S., Borenstein, J., Koka, R., Lalan, S., Ochoa, E. R., Ravens, M., Pien, H., Cunningham, B., and Vacanti, J. P. (2000) Silicon micromachining to tissue engineer branched vascular channels for liver fabrication. *Tissue Eng.* **6,** 105–117

33. Neumann, T., Nicholson, B. S., and Sanders, J. E. (2003) Tissue engineering of perfused microvessels. *Microvasc. Res.* **66,** 59–67

Received August 6, 2005; accepted December 5, 2005.

Fig. 1

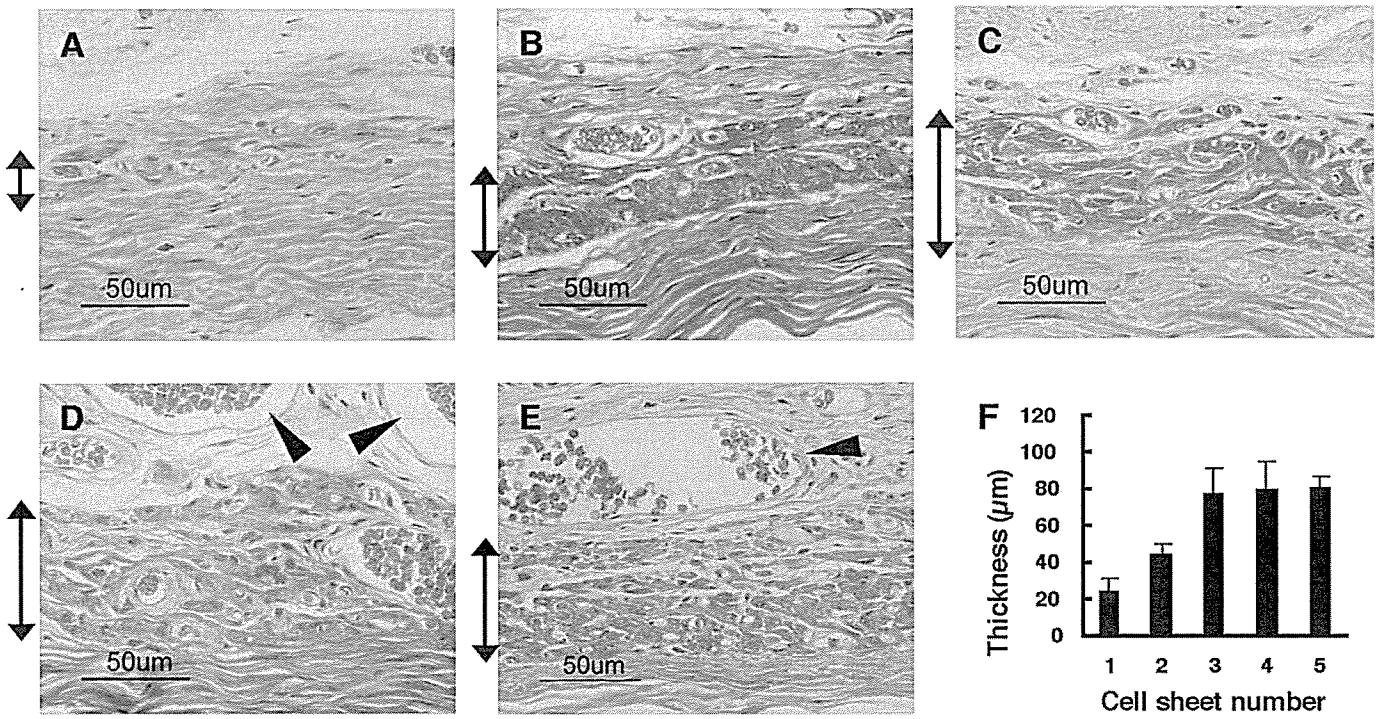

Figure 1. Mass transport limitations of transplanted tissues due to acute ischemia. Increasing numbers (1–5) of cardiomyocyte sheets were transplanted into subcutaneous tissue and fixed at 4 wk. Azan staining shows viable laminar myocardial tissues for the cases of 1 (***A***), 2 (***B***), and 3 layer (***C***) constructs. Necrotic areas including disordered vascular networks (black arrowheads) and connective tissues are observed in the 4 (***D***) and 5 layer (***E***) cases. Bidirectional arrows indicate viable cell sheet layers. Orange-stained red blood cells indicate the presence of vasculature. ***F***) Graph shows that final tissue thickness of transplanted grafts increased linearly up to 3 layer constructs, and plateaus in 4 and 5 layer constructs (25±6, 44±6, 78±14, 80±16, and 83±5 μm thicknesses, respectively). Data are mean ± SD (n=4).

Fig. 2

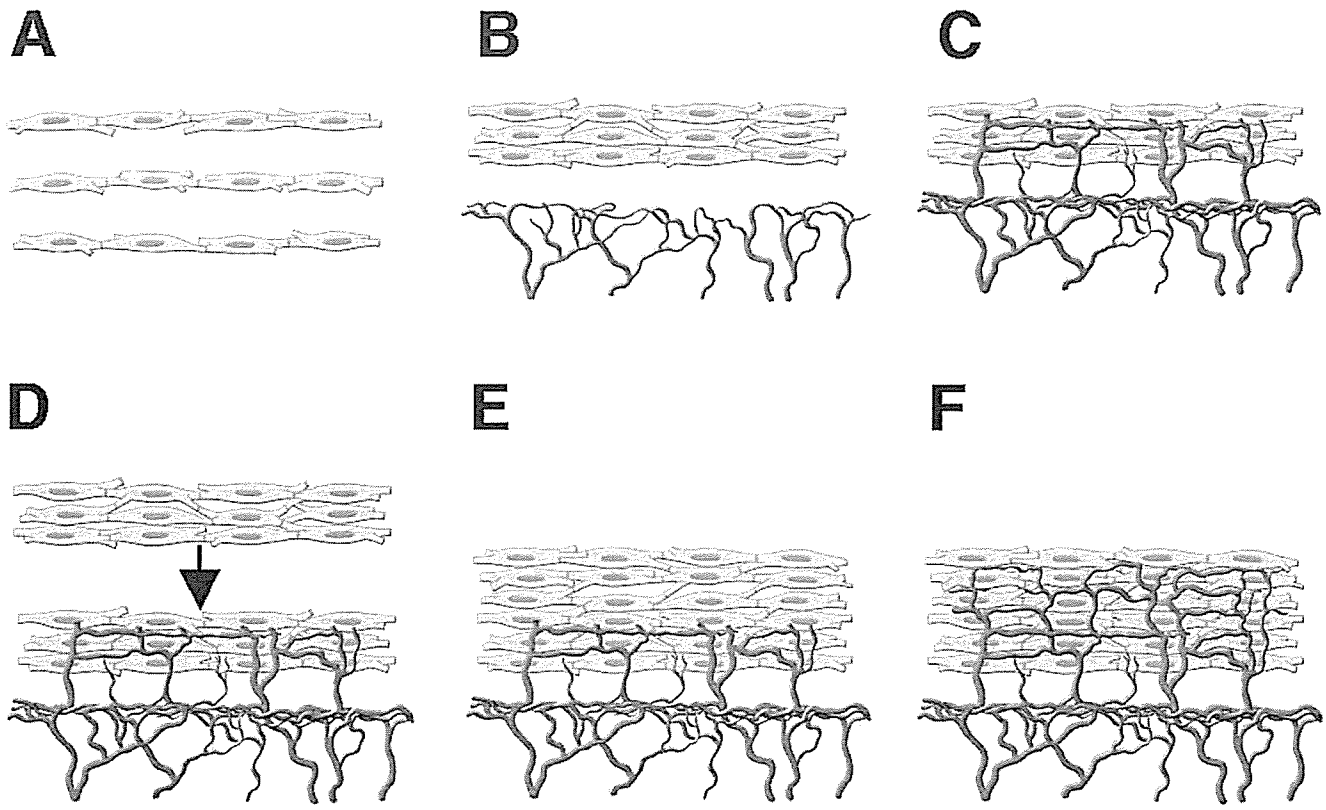

Figure 2. Schematic illustration of polysurgery to bioengineer vacularized cell-dense tissues. ***A, B***) Three confluent cell sheets are stacked as the initial graft and then transplanted in vivo. ***C***) While the graft initially survives based solely on nutrient diffusion, sufficient growth of microvascular networks ultimately occurs within the first graft in a few days. ***D, E***) Afterward, a second triple layer graft is overlaid on the first. ***F***) The resulting multilayer cell-dense tissue construct is now perfused through both layers by underlying microvasculature.

Fig. 3

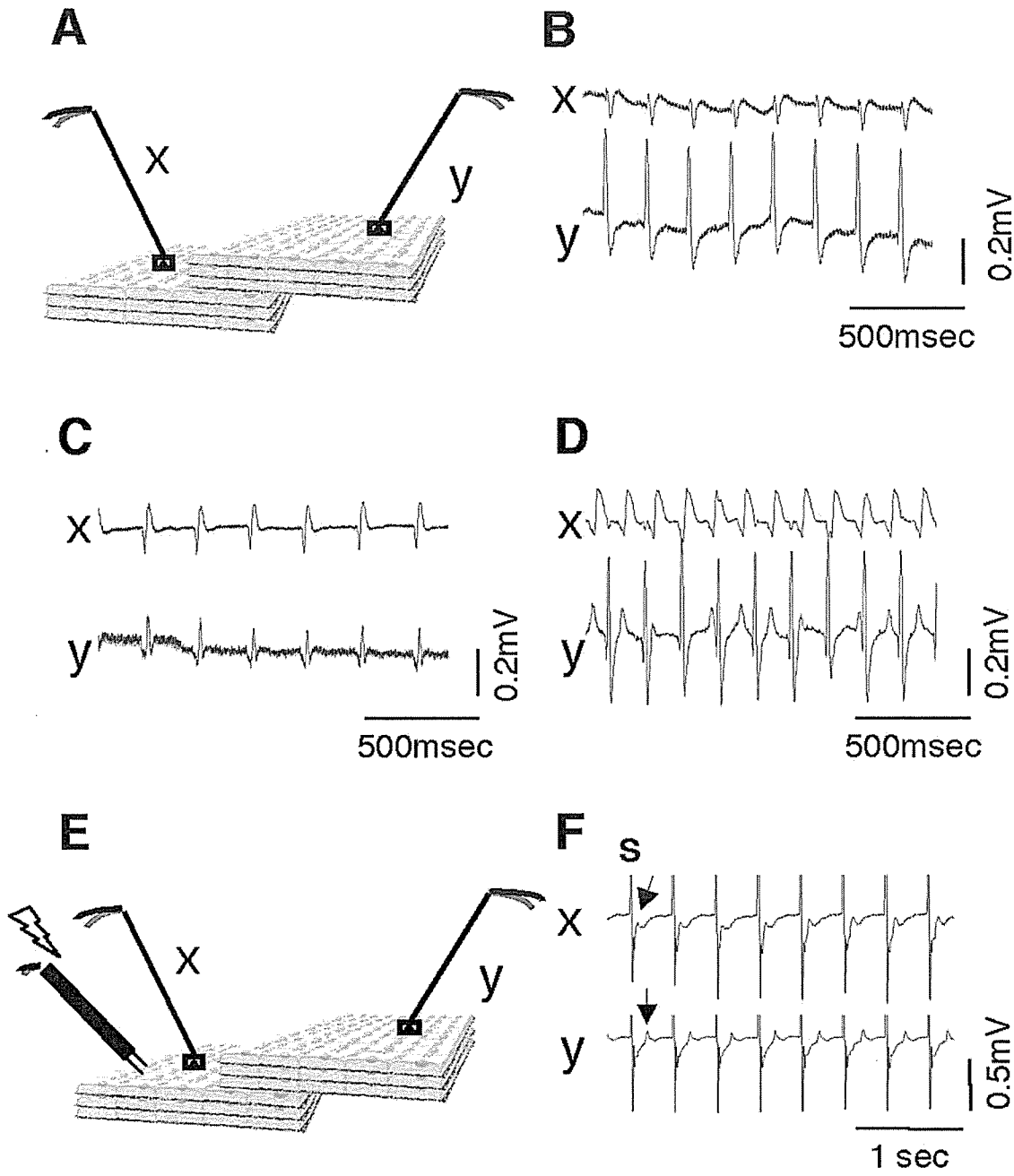

Figure 3. Electrophysiological communication between overlaid myocardial tissue grafts. ***A***) Schematic illustration of electrical analyses shows 2 triple-layer grafts were partially overlaid at 1, 2, or 3 day intervals in rat dorsal subcutaneous tissues. One month after these procedures, transplantation sites were opened and two electrodes (x and y) were placed over single parts of exposed grafts in vivo. ***B–D***) Representative tracings of detected electrical potentials are shown. Electrical potentials of spontaneously beating grafts demonstrate complete synchronization in the cases of 1 day (***B***) or 2 day (***C***) polysurgery intervals, but asynchrony in the case of the 3 day interval (***D***). ***E***) A stimulation bipolar electrode was set at the edge of one graft, and monophasic pacing pulses (2–4 Hz, 5 ms, 2–3 V) were applied to examine electrical communication between grafts. Evoked electrical potentials were detected with 2 electrodes set over a single part of each graft (x and y). ***F***) Electrical stimulation, which was applied overlaid myocardial tissue grafts (using 1 day interval), was transmitted from one graft (x) to the other (y). S indicates stimulation. Arrows indicate evoked electrical potentials.

Fig. 4

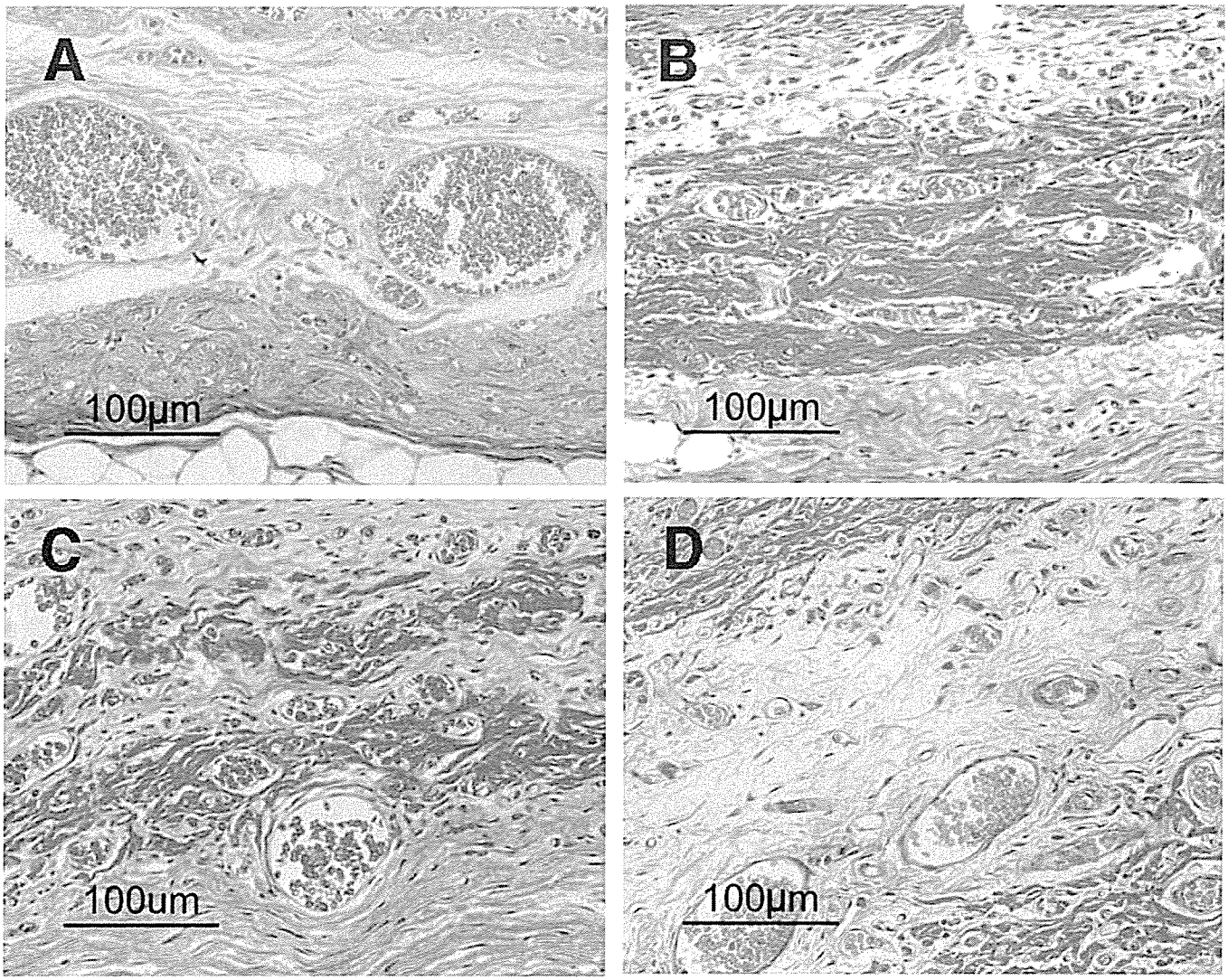

Figure 4. Morphological communication between overlaid myocardial tissue grafts. Azan staining of the various 6-layer constructs is compared. ***A***) Significant necrotic tissue including replacement of normal tissue by large areas of vascularized tissue is observed in the construct created by single-step procedure. ***B***) In the case of polysurgery at 1 day intervals, intimate connectivity of the two grafts was observed, with surviving, full-thickness tissue complete with microvascular network formation. ***C***) In the case of 2 day tandem transplant intervals, some separation of the two grafts by connective tissue is seen. ***D***) Completely dissociated grafts are observed with the 3 day transplant interval.

Fig. 5

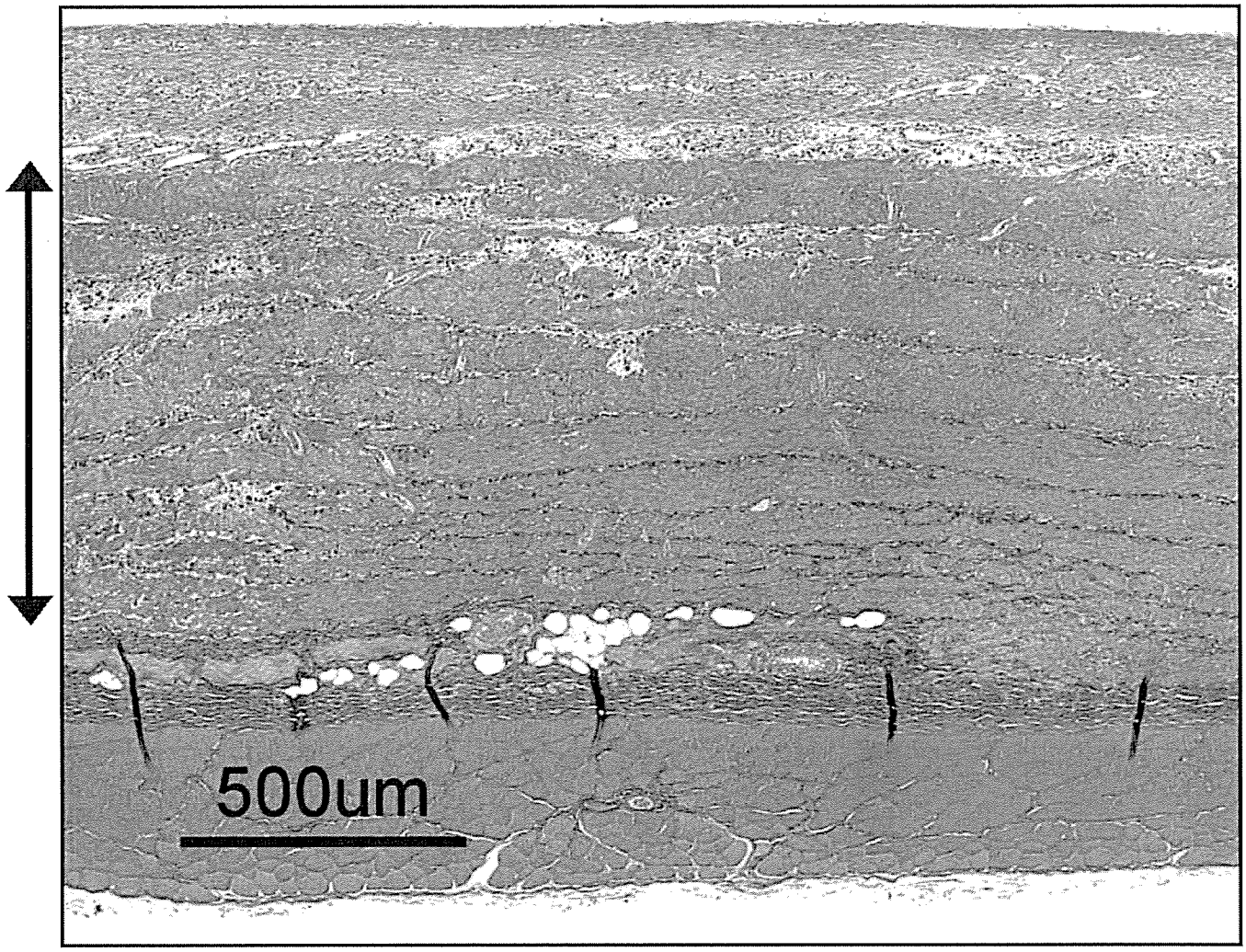

Figure 5. Thick cell-dense tissues engineered using 10-times polysurgery. Azan staining shows that by using 10-times polysurgery with 1 day intervals, multilayer cell-dense myocardium with well-organized microvessels can be created. Bidirectional arrow indicates viable myocardial cell sheet layers. The measured thickness of the grafts was 0.84 ± 0.16 mm. Data are mean ± SD (n=3).

Fig. 6

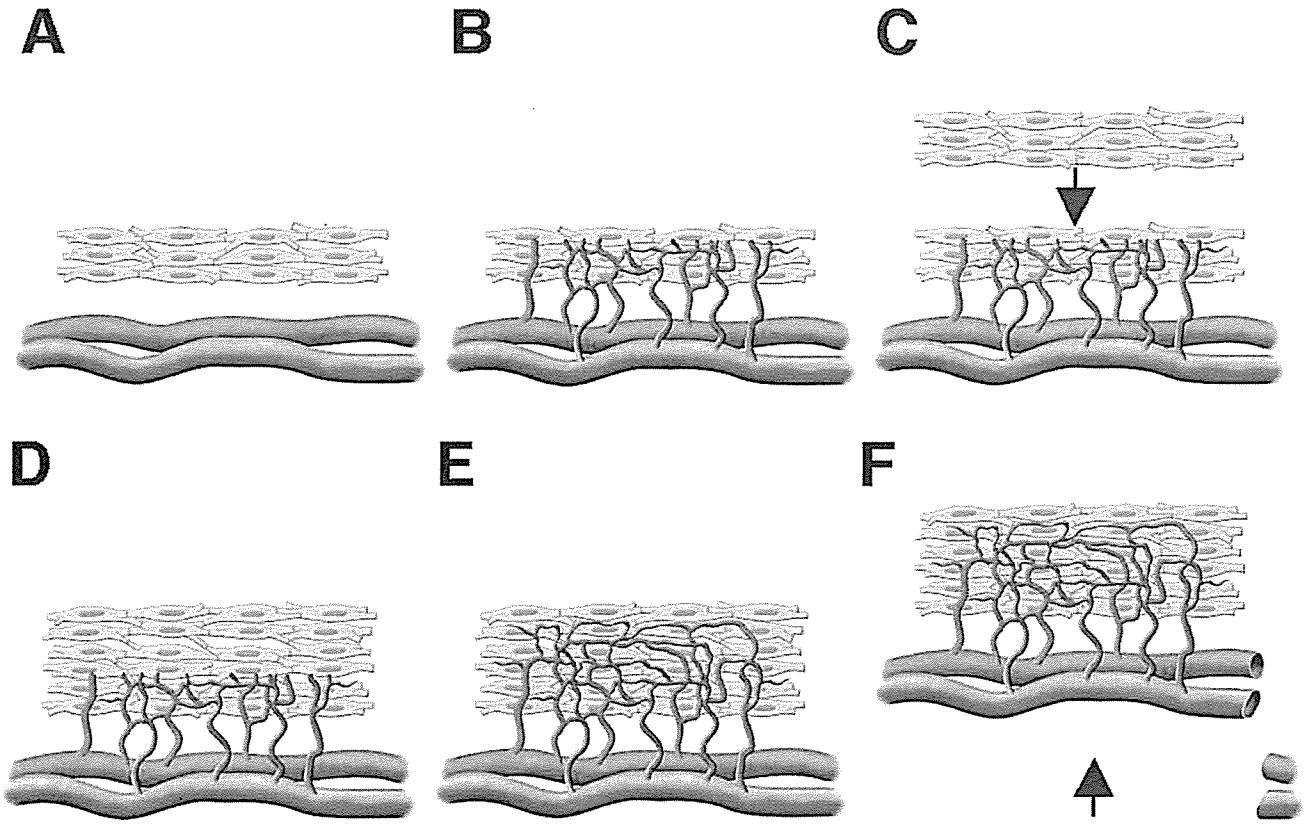

Figure 6. Schematic illustration of the concept used for bioengineering multilayer grafts with surgically connectable vessels. ***A***) First graft is transplanted over a surgically accessible artery and vein. ***B***) In this case, the graft is supplied with both new vasculature and blood directly from these existing vessels. ***C, D***) After sufficient vascularization has occurred, second graft is transplanted onto the first graft. ***E, F***) Finally, the microvascularized construct accompanied by graftable vessels harvested from the host is fully perfused by host vessels and surgically resected. Ectopic transplantation of such a graft is then possible.

Fig. 7

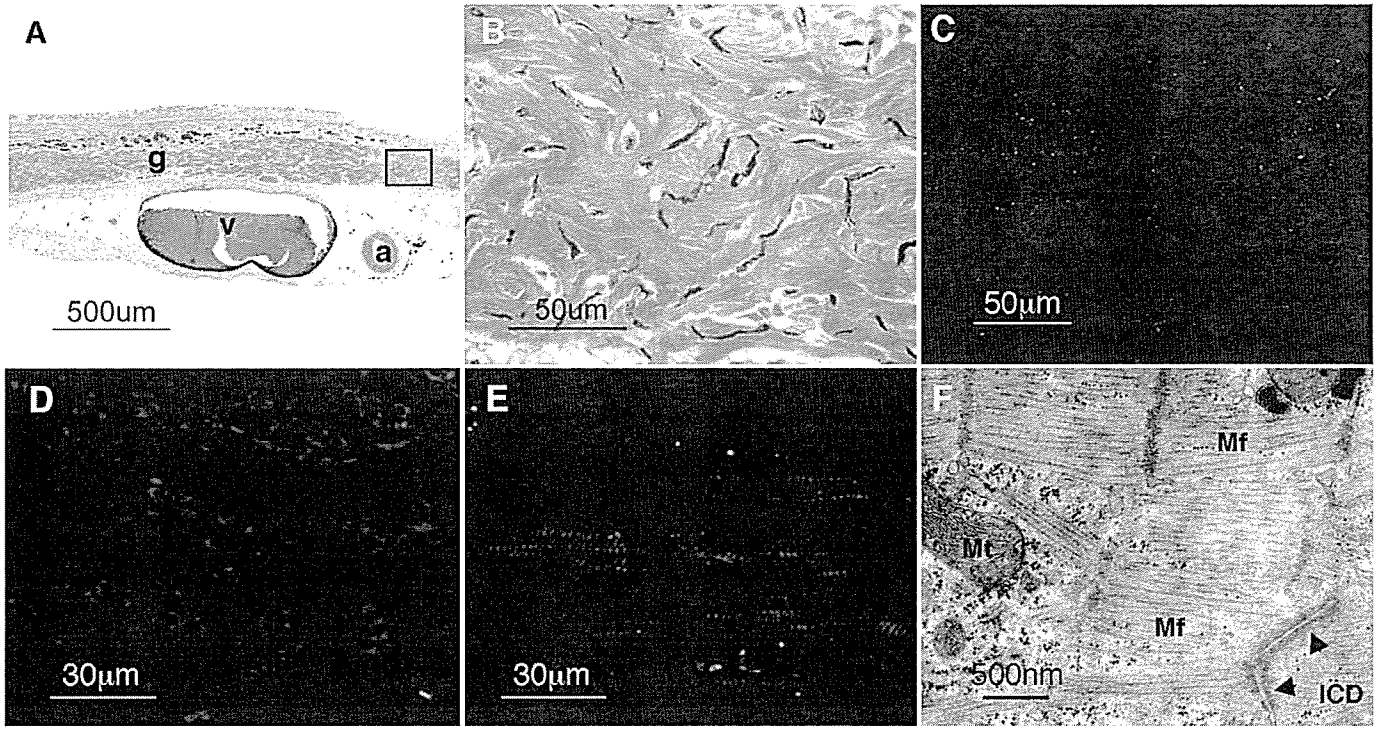

Figure 7. Myocardial tissue grafts created over surgically accessible blood vessels. ***A***) Azan staining shows multilayer myocardial tissue graft (g) over the caudal epigasiric artery (a) and vein (v) which was fixed 2 wk after the polysurgery procedure described. Black ink injected from host femoral artery stains vasculature within and surrounding graft. ***B***) Under high magnification, area of tissue as indicated by square box in ***A*** shows complete microvascular networks within construct, which are stained with black ink, indicating blood supply to construct via the selected artery. ***C***) Immunohistochemistry for connexin 43 shows diffuse staining throughout the entire myocardial tissues, suggesting gap junction formation within the bioengineered constructs. ***D***) Anti-troponin T antibody staining demonstrated diffuse and disorganized staining at 3 days after transplantation. ***E***) On the other hand, cardiomyocytes were striated and sarcomeres were well organized in myocardial tissue graft at 7 days. ***F***) TEM results at 7 days showed characteristic structures of myocardium including well-organized myofilaments (Mf), mitochondria (Mt), and intercalated disks (ICD).

J Bone Miner Metab (2005) 23:337–340
DOI 10.1007/s00774-005-0610-y

MINI REVIEW

**Toshiyuki Ikeda · Hiroshi Kawaguchi · Satoru Kamekura
Naoshi Ogata · Yoshiyuki Mori · Kozo Nakamura
Shiro Ikegawa · Ung-il Chung**

Distinct roles of Sox5, Sox6, and Sox9 in different stages of chondrogenic differentiation

Received: February 18, 2005 / Accepted: April 3, 2005

Key words Cartilage · Formation · Regeneration · Sox

Introduction

In mammals, most skeletal elements are formed through endochondral bone formation, which is characterized by the initial formation of cartilage molds from mesenchymal condensations and their subsequent replacement by bones [1]. A small number of skeletal elements, including some craniofacial bones, are formed through intramembranous bone formation, which is characterized by direct transformation of mesenchymal condensations into bones. During the initial step common to both processes, the mesenchyme receives patterning signals that determine the shape, size, and number of mesenchymal condensations [2]. Molecules providing such patterning information are members of the Wnt, hedgehog, and fibroblast growth factor (FGF) families, and the TGF-β superfamily, a series of transcription factors of the Hox, Pax, homeodomain-containing, Forkhead, and basic helix–loop–helix (bHLH) families, and of cell adhesion molecules, including N-cadherin and NCAM [3]. During the endochondral process, cells in the mesenchymal condensations differentiate into chondrocytes, while cells at the periphery become perichondrial cells [4]. Chondrocytes, the primary cell type of cartilage, have a characteristic shape, express a characteristic genetic program, and deposit a characteristic extracellular matrix rich in type II collagen and the proteoglycan aggrecan. The cartilage enlarges through chondrocyte proliferation and matrix production. Subsequently, chondrocytes in the center of the cartilage stop proliferating, dramatically increase in size (hypertrophy), and change their genetic program to synthesize a matrix rich in type X collagen. Hypertrophic chondrocytes play a pivotal role in coupling chondrogenesis and osteogenesis in the endochondral process; they mineralize a surrounding matrix to provide a scaffold for osteoblasts, direct adjacent cells in the perichondrium and the primary spongiosa to become osteoblasts, and attract blood vessels and blood cells, including osteoclasts [5,6]. Hypertrophic chondrocytes then undergo apoptotic cell death. The pathways of chondrocyte and osteoblast differentiation are thus coordinated in time and space during endochondral bone formation. This review summarizes the roles of Sox5, Sox6, and Sox9 in the different steps of chondrogenic differentiation.

T. Ikeda · N. Ogata · Y. Mori · U.-i. Chung (✉)
Division of Tissue Engineering, University of Tokyo Hospital, 7-3-1 Hongo, Bunkyo-ku, Tokyo 113-8655, Japan
Tel. +81-35-800-9891; Fax +81-35-800-9891
e-mail: uichung-tky@umin.ac.jp

H. Kawaguchi · S. Kamekura · K. Nakamura
Division of Motor and Sensory System Medicine, University of Tokyo Hospital, Tokyo, Japan

S. Ikegawa
SNP Research Center, RIKEN, Tokyo, Japan

Roles of Sox9 in chondrogenesis

Sox9 is a member of the Sox family of transcription factors, which are characterized by a high-mobility-group (HMG)-box DNA-binding domain, whose sequence is at least 50% identical with that of the sex determining factor SRY [7]. The Sox family is composed of several subgroups based on sequence homologies both inside and outside the HMG-box domain [8]. Sox9 has a transcription activation domain and binds to a specific sequence in the minor groove of DNA [9]. Sox9 efficiently binds to single and double HMG-box sites in DNA. In mouse embryos, Sox9 is expressed in all chondroprogenitor cells and all chondrocytes, while its expression is dramatically decreased in hypertrophic chondrocytes [10–12].

Physiological roles of Sox9 in chondrogenesis were first demonstrated by the human genetic disease campomelic dysplasia (CD). This disease is caused by heterozygous inactivating mutations in and around the *SOX9* gene and is characterized by hypoplasia of all endochondral skeletal

elements [13,14]. Heterozygous *Sox9* mutant (*Sox9+/–*) mice phenocopied CD in the skeletal phenotype, supporting the human data. In *Sox9+/–* mouse embryos, smaller and delayed mesenchymal condensations caused the hypoplasia of endochondral bones and elongation of the hypertrophic layer of the growth plate and premature mineralization in several bones [15]. Taken together, these data suggest that Sox9 negatively regulates the transition of chondrocyte proliferation into hypertrophy. Since no homozygous *Sox9* (*Sox9–/–*) mutants could be generated, owing to the perinatal lethality and sex reversal of *Sox9+/–* mice, the effects of a complete loss of Sox9 on chondrogenesis were examined in mouse chimeras containing both *Sox9–/–* and wild-type cells by injecting *Sox9–/–* embryonic stem (ES) cells into wild-type blastocysts [16]. While *Sox9–/–* and wild-type cells were intermingled in chondrogenic fields prior to the formation of mesenchymal condensations, *Sox9–/–* cells were excluded from chondrogenic mesenchymal condensations and never expressed chondrocyte marker genes such as *Col2a1*, *Col9a2*, *Coll1a2*, and *aggrecan*. In addition, in teratomas derived from *Sox9–/–* ES cells, no cartilage formed. Inactivation of the *Sox9* gene in limb buds using the Cre recombinase/loxP recombination system before chondrogenic mesenchymal condensations resulted in the complete absence of mesenchymal condensations with abolished expression of chondrocyte marker genes [17]. These data demonstrate an important role of Sox9 in the initial step of chondrogenesis, that is, mesenchymal condensations (Fig. 1).

Chondrocyte-specific enhancers of the *Col2a1*, *Coll1a2*, and *CDRAP* genes contain Sox9 binding sites [9,10,18,19]. These enhancers were activated by Sox9 in transfection experiments and also in vivo for the *Col2a1* enhancer [20]. In addition, enhancer mutations that abolished DNA binding of Sox9 inactivated these enhancers in vivo. These data suggest that Sox9 has a role in regulating chondrocyte marker genes after mesenchymal condensations. When Sox9 was deleted by using the Cre recombinase/loxP recombination system after chondrogenic mesenchymal condensations, severe generalized chondrodysplasia occurred with a severe reduction of cartilage-specific matrix production and lack of proliferating chondrocytes [17]. These data demonstrate an important role of Sox9 in chondrogenesis after mesenchymal condensations as well (Fig. 1).

The expression and function of Sox9 is not restricted to chondrogenesis [13,14], suggesting that other transcription factors may cooperate with Sox9 to specifically activate chondrocyte marker genes. Other Sox proteins interact with transcription factors of different families, and those interactions may increase the specificity of these Sox proteins in activating target genes [21–23].

Roles of Sox5 and Sox6 in chondrogenic differentiation

Sox5 and Sox6, which have a high degree of sequence identity with each other, belong to a different subgroup of Sox proteins and present no sequence homology with Sox9 except for the HMG-box. Sox5 and Sox6 are coexpressed with Sox9 during chondrogenic differentiation [24]. Both genes are expressed in several nonchondrogenic tissues [25]. Owing to the presence of a highly conserved coiled-coil domain, Sox5 and Sox6 form homodimers and heterodimers with each other, which bind much more efficiently to pairs of HMG-box binding sites than to single binding sites. Unlike Sox9, Sox5 and Sox6 do not contain a transcriptional activation domain. Sox5 and Sox6 cooperate with Sox9 to activate the *Col2a1* enhancer and the *Col2a1* and *aggrecan* genes in vitro.

Physiological roles of Sox5 and Sox6 in chondrogenic differentiation were demonstrated by genetically manipulated mice. Although homozygous *Sox5* mutant (*Sox5–/–*) mice and *Sox6* mutant (*Sox6–/–*) mice were born with relatively mild skeletal anomalies, double mutant

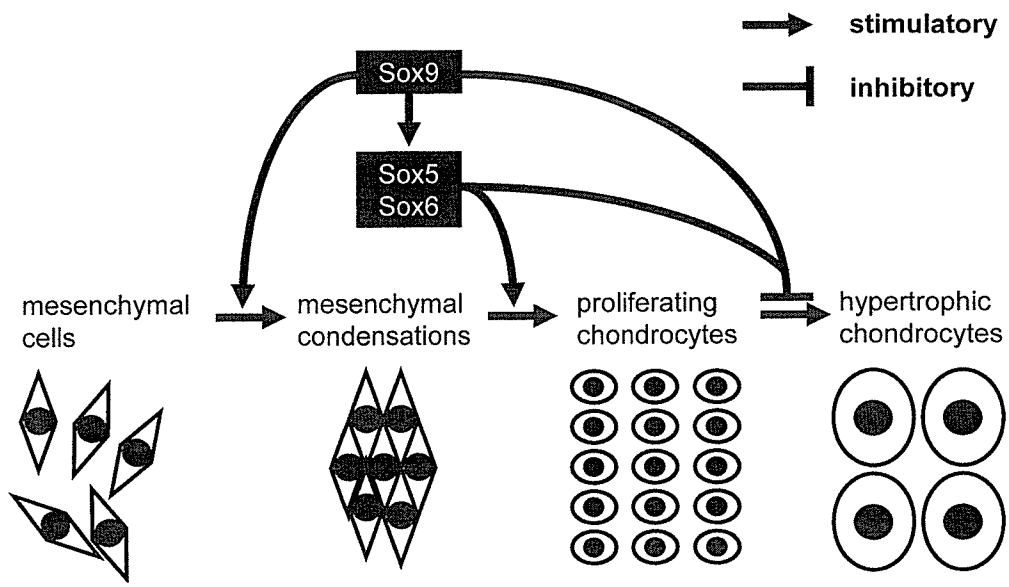

Fig. 1. Diagram of the actions of Sox5, Sox6, and Sox9 in different steps of chondrogenic differentiation